Analysis of voltage output LCC resonant converters, including boost mode operation

H.I. Sewell, M.P. Foster, C.M. Bingham, D.A. Stone, D. Hente and D. Howe

Abstract: A novel methodology for the high-speed analysis of LCC voltage output resonant power converters is presented. Termed rectifier transformed fundamental mode analysis, the procedure employs describing functions for determining equivalent passive circuit models for the combined rectifier, output filter and load circuitry. The resulting passive network is then used to predict voltages and currents throughout the converter. A refinement algorithm is also described that further enhances the accuracy of the analysis. Unlike previously published techniques, the proposed procedure is shown to accurately predict converter operation in the boost mode; a mode that normally requires the incorporation of an additional step-up transformer to realise output voltages that are higher than the input voltage in the converter topology under consideration. The accuracy of the procedure, and the enhancement that results from the refinement process, is demonstrated by comparing predictions of the maximum output voltage of LCC converters as a function of load, and the regulation at a fixed switching frequency as a function of the parallel rectifier capacitance with measurements from prototype converters, including operation in boost mode. The results confirm that the methodology is capable of correctly predicting the steady-state behaviour of voltage output LCC series resonant converters, particularly around the resonant frequency where previously published techniques can exhibit significant error.

List of symbols

i_{in}	time-varying input current to resonant circuit
I_{in}	peak input current to resonant circuit
C_s	series resonant capacitor
L_s	series resonant inductor
f_s	switching frequency
C_p	parallel capacitor across rectifier input
v_{rect}	time-varying voltage at input to rectifier
r_l	fundamental made analysis equivalent load resistor
V_{out}	DC output voltage
V_{diode}	diode on-state voltage drop
V_{eq}	FMA equivalent supply voltage
V_{DC}	DC supply voltage
r_η	rectifier transformed fundamental mode analysis (RTFMA) derived resistor to account for effect of C_p
c_η	RTFMA derived capacitor to account for effect of C_p
v_{r0}	offset voltage for integration
V_b	peak bridge rectifier voltage
δ_1	time at which bridge begins to conduct
I_{out}	output DC current
v_{sq}	time domain square-wave component of v_{rect}
v_η	time domain η-shaped component of v_{rect}
V_{sq}	RTFMA equivalent of v_{sq}
r_{sq}	RTFMA equivalent resistor modelling square-wave component of v_{rect}
V_η	RTFMA equivalent of v_η
$\gamma_{1\ldots4}$	intermediate variables
r'_{eq}	initial estimate of resistance from RTFMA model
c'_η	initial estimate of circuit capacitance from RTFMA model of V_η
c'_{tot}	initial estimate of total circuit capacitance from RTFMA
I'_{in}	initial estimate of peak input current
f_{0eff}	effective resonant frequency
Q_{0eff}	effective quality factor
Z_{0eff}	effective impedance of resonant circuit
θ	normalised event angle
θ_1	event angle at which rectifier begins to conduct

1 Introduction

The ever-increasing demand for smaller and more efficient power supplies for compact electronic equipment has led to a resurgence of interest in resonant power converters. Moreover, the enhanced attributes of switching high-order tank circuits are focusing attention to more complex resonant circuitry [1–4]. Increased complexity, however, makes it more difficult to accurately predict performance during the design process due to the protracted simulation times required by component-based simulation packages, such as SPICE.

A method that facilitates the high-speed analysis and synthesis of voltage output resonant mode DC-DC converters with a capacitor across the rectifier, as illustrated in Fig. 1, is presented. Although the current output counterpart, that incorporates an additional inductor in the output filter circuit, may be favoured for high power applications due to the lower current ripple, the voltage output converter topology is often preferred for low power

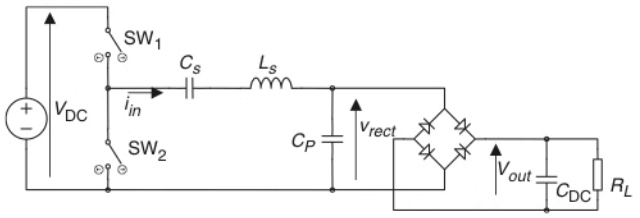

Fig. 1 *Converter topology*

applications since it has fewer reactive components, and, hence, reduced circuit complexity and lower cost.

The inclusion of the capacitor, C_p across the input to the bridge rectifier in Fig. 1 allows the distributed interturn capacitance of an isolating transformer, and the parasitic capacitance of the rectifier to be accounted for in the analysis and design of the converter. Moreover, it will be shown that C_p can be utilised to enable the converter to provide a boost operating mode; a feature that is not possible with standard second-order LC series converters with a voltage output, and which has not previously been reported.

Until recently, rapid analysis of higher-order voltage output converters has been resistant to high speed fundamental mode analysis (FMA), in which the rectifier, output filter and load are replaced by an equivalent series resistor, r_l (Fig. 2), and recourse has had to be made to time-domain multidimensional design curves. Recently, however, rectifier compensated fundamental mode analysis (RCFMA), has emerged, that models the interaction between the rectifier and resonant components by an equivalent set of second-order components along with the classical FMA series resistor, r_l [5]. Although RCFMA has been shown to significantly improve prediction accuracy compared to traditional FMA, accuracy is known to deteriorate around the resonant frequency, and also for converters designed for low output voltages as a consequence of not explicitly accounting for the effect of the bridge-rectifier voltage drop.

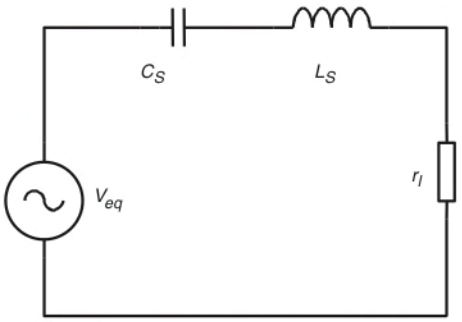

Fig. 2 *Classic FMA equivalent circuit*

In this paper, alternative describing functions that model the nonlinear interaction between the rectifier and the parallel capacitor, C_p, are derived, initially yielding complex equivalent voltage sources, V_{sq} and V_η, as shown in Fig. 3. A transformation of the equivalent voltage sources then provides equivalent passive components, r_{sq}, C_η and r_η, that reduce the analysis of the complex operation of the converter to that of a simple passive network (Fig. 4). A refinement procedure is then used to enhance the accuracy of the resulting analyses. An additional benefit of the proposed technique is that it facilitates an accurate estimate of the output voltage of the converter from the measured current in the resonant network; a feature that can be employed to reduce the cost of sensing the output voltage in isolated systems.

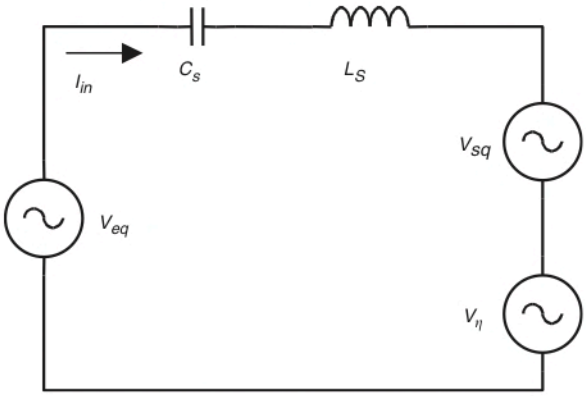

Fig. 3 *RTFMA equivalent circuit*

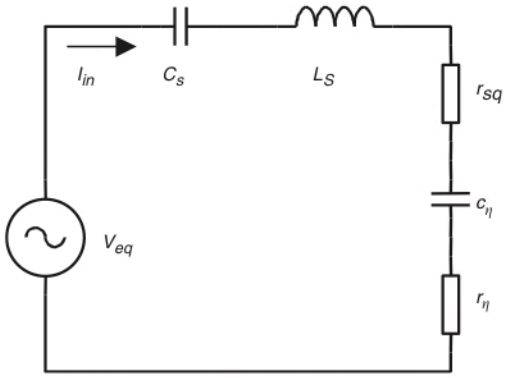

Fig. 4 *Transformed RTFMA equivalent circuit*

2 Fundamental mode analysis

A consequence of employing FMA for the analysis of power electronic converters is that the current, i_{in}, which flows through the series resonant network (comprised of C_s and L_s) must be assumed to be sinusoidal (1)

$$i_{in} = I_{in}\sin(2\pi f_s t) \tag{1}$$

If the nonlinear effect of the capacitor, C_p, across the bridge rectifier, can be disregarded, the voltage across the bridge rectifier, v_{rect}, would be a square wave with a magnitude given by the sum of the output voltage and the diode voltage drops (2)

$$v_{rect} = (V_{out} + 2V_{diode})\mathrm{sgn}(i_{in}) \tag{2}$$

If the diode voltage drops are neglected, the standard describing function for the rectifier and output circuit is modelled by a fixed resistor, r_l, (3) [1]

$$r_l = \frac{8}{\pi^2}R_L \tag{3}$$

The DC-link voltage and power switches are modelled as an effective sinusoidal voltage with a peak value, V_{eq}, given by (4). The switches are assumed to provide an ideal square wave voltage with commutation effects ignored [1]

$$V_{eq} = \frac{2}{\pi}V_{DC} \tag{4}$$

Thus, an AC equivalent circuit can be obtained (Fig. 2) and used for analysis, the output power being inferred from the dissipation in the equivalent load resistance, r_l. This procedure constitutes the classical FMA of resonant DC-DC converters.

3 Rectifier transformation

If the addition of parallel capacitor C_p is such that dv_{rect}/dt may not be neglected, the direct component mapping (3) is no longer adequate for accurate analysis. Thus, a modified equivalent circuit (Fig. 4) is proposed that incorporates an additional resistance r_η and a series capacitance C_η, to account for the significant effects of the charge/discharge times of C_p.

In general, the presence of C_p causes the waveform of v_{rect} to depart from a square wave (see Fig. 5, for example). At the zero-crossing times of i_{in}, conduction of the bridge rectifier ceases, and i_{in} begins charging C_p until $|v_{rect}|$ equals the sum of the output voltage and the on-state voltage drop of the bridge rectifier, at which time the bridge rectifier again begins to conduct. Since operation of the converter in the steady-state is cyclic, event timings can be replaced by event angles, thereby removing the need to explicitly denote each operational mode as part of an infinite series. The mapping of an event time, δ, to the equivalent angle, θ, is given by (5)

$$\theta = 2\pi f_s \delta \bmod 2\pi \tag{5}$$

During the period when C_p is being charged, its voltage varies as the integral of the charging current, as given in (6), in which the offset, v_{r0}, is included as the initial condition, and where $v_{r0} = \pm(V_{out} + 2\mathrm{V}_{doide})$.

$$v_{rect} = v_{r0} + \frac{1}{C_p}\int_0^{\delta} I_{in}\sin(2\pi f_s t)dt \quad t = 0 \ldots \delta_1 \tag{6}$$

Solving for v_{rect} for the case when $v_{r0} = -(V_{out} + 2V_{diode})$ gives

$$v_{rect} = -V_b + \frac{I_{in}}{2\pi f_s C_p}(1 - \cos(2\pi f_s t)) \tag{7}$$

where $V_b = V_{out} + 2V_{diode}$.

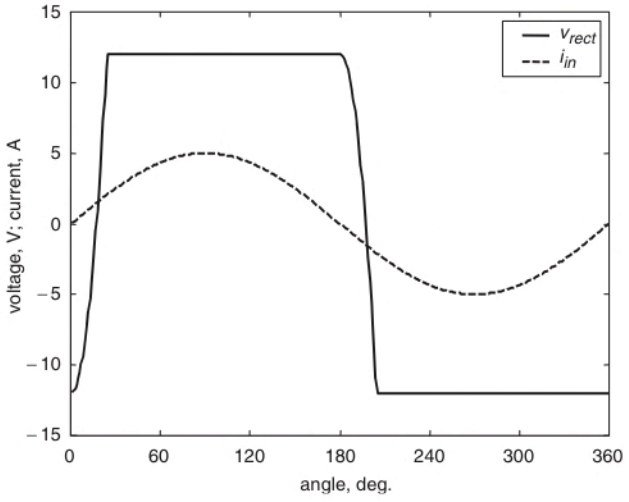

Fig. 5 *Example of time-domain voltage across rectifier*

The boundary time that defines the end of the charging period is determined by substituting $v_{rect} = V_b$ into (7) and solving for $t = \delta_1$, giving

$$\delta_1 = \frac{1}{2\pi f_s}\cos^{-1}\left(1 - \frac{4\pi V_b f_s C_p}{I_{in}}\right) = \frac{1}{2\pi f_s}\theta_1 \tag{8}$$

and from (5)

$$\theta_1 = \cos^{-1}\left(1 - \frac{4\pi V_b f_s C_p}{I_{in}}\right) \tag{9}$$

The definition of v_{rect} for the half-cycle, $\theta = 0 \rightarrow \pi$, is therefore

$$v_{rect} = \begin{cases} -V_b + \dfrac{I_{in}}{2\pi f_s C_p}(1 - \cos(\theta)) & \theta = 0 \ldots \theta_1 \\ V_b & \theta = \theta_1 \ldots \pi \end{cases} \tag{10}$$

At $\theta = \pi$, the current reverses, the rectifier bridge ceases to conduct, and the input current, i_{in}, discharges C_p from V_b to $-V_b$, at which time v_{rect} is clamped at $-V_b$ until $\theta = 2\pi$. The negative half-cycle is, therefore, the mirror image of the positive half-cycle, and, when combined, are described by (11) (see Fig. 5)

$$v_{rect} = \begin{cases} -V_b + \dfrac{I_{in}}{2\pi f_s C_p}(1 - \cos(\theta)) & \theta = 0 \ldots \theta_1 \\ V_b & \theta = \theta_1 \ldots \pi \\ V_b - \dfrac{I_{in}}{2\pi f_s C_p}(1 + \cos(\theta)) & \theta = \pi \ldots \pi + \theta_1 \\ -V_b & \theta = \pi + \theta_1 \ldots 2\pi \end{cases} \tag{11}$$

3.1 Output current

The output current from the converter can be determined by calculating the average current which passes through the bridge rectifier during a complete cycle. Defining the angle at which the bridge rectifier starts to conduct as θ_1, the average current is found by integration from

$$I_{out} = \frac{1}{2\pi}\left\{\int_{\theta_1}^{\pi} I_{in}\sin(\theta)d\theta + \int_{\theta_1+\pi}^{2\pi} -I_{in}\sin(\theta)d\theta\right\} \tag{12}$$

where the polarity inversion in the second integral is due to the bridge rectifier reversing the input current, giving

$$I_{out} = \frac{2}{\pi}(I_{in} - 2\pi V_b f_s C_p) \tag{13}$$

3.2 Output voltage

The output voltage from the converter is calculated by assuming an infinite filter capacitance i.e. $C_{DC} \rightarrow \infty$, in which case knowledge of I_{out} and Ohm's law provides

$$V_{out} = R_L I_{out} \tag{14}$$

Alternatively, substituting V_b from (7) into (13), and the result into (10), the output voltage can be calculated as a function of the input current (15)

$$V_{out} = \frac{2R_L I_{in}}{\pi(1 + 4R_L f_s C_p)} \tag{15}$$

4 Determination of equivalent passive components

The voltage across the capacitor at the input to the bridge rectifier (11) shown in Fig. 5, can be subdivided into the sum of two components; viz. a square-wave voltage which is in phase with the current, and a η-shaped waveform, as illustrated in Fig. 6, i.e.

$$v_{rect} = v_{sq} + v_\eta \tag{16}$$

By appropriate transformation, it is now shown how the constituents of v_{rect} can be modelled by an equivalent resistance and capacitance to facilitate accurate and rapid analysis of the converter.

4.1 Equivalent passive component modelling v_{sq}

The equivalent FMA source of v_{sq} can be found from the fundamental of the Fourier series, having been described in

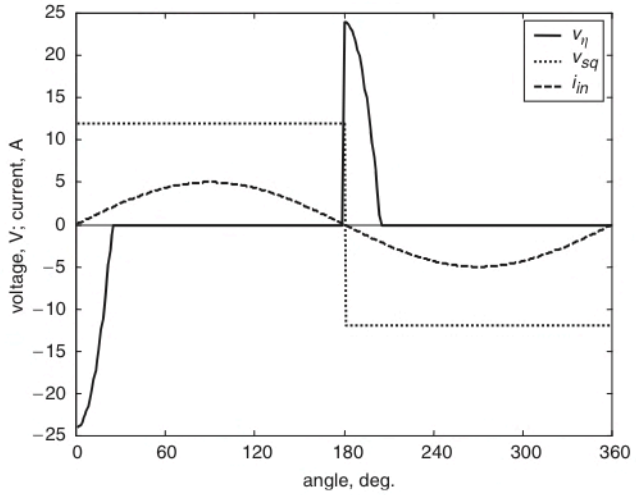

Fig. 6 *Example of time-domain voltage across rectifier due to rectifier action and parallel capacitor*

each half-cycle by

$$v_{sq} = \begin{cases} V_b & \theta = 0 \ldots \pi \\ -V_b & \theta = \pi \ldots 2\pi \end{cases} \tag{17}$$

where V_b can be described in terms of I_{in} by substituting (15) into (7) and simplifying

$$V_b = \frac{2R_L I_{in} + 2V_{diode}}{\pi(1 + 4R_L f_s C_p)} \tag{18}$$

The FMA equivalent voltage source can then be found by taking the fundamental of the Fourier series, as follows:

$$\begin{aligned} v_{sq} = &\frac{1}{2\pi}\int_0^{\pi}\left(\frac{2R_L I_{in} + 2V_{diode}}{\pi(1 + 4R_L f_s C_p)}\right)\sin(\theta)d\theta \\ &+ \frac{1}{2\pi}\int_{\pi}^{2\pi}\left(-\frac{2R_L I_{in} + 2V_{diode}}{\pi(1 + 4R_L f_s C_p)}\right)\sin(\theta)d\theta \\ &+ j\left[\frac{1}{2\pi}\int_0^{\pi}\left(\frac{2R_L I_{in} + 2V_{diode}}{\pi(1 + 4R_L f_s C_p)}\right)\cos(\theta)d\theta\right. \\ &\left.+ \frac{1}{2\pi}\int_{\pi}^{2\pi}\left(-\frac{2R_L I_{in} + 2V_{diode}}{\pi(1 + 4R_L f_s C_p)}\right)\cos(\theta)d\theta\right] \end{aligned}$$

On evaluation of the integrals, and simplifying, the FMA equivalent voltage source is given by

$$v_{sq} = \frac{8(R_L I_{in} + \pi V_{diode} + 4\pi f_s C_p V_{diode} R_L)}{\pi^2(1 + 4R_L f_s C_p)} \tag{19}$$

Since v_{sq} is in phase with the input current, by rearrangement, v_{sq} can be represented by an equivalent resistance, r_{sq}

$$r_{sq} = \frac{8R_L}{\pi^2(1 + 4R_L f_s C_p)} + \frac{8V_{diode}}{I_{in}\pi} \tag{20}$$

4.2 Equivalent passive component modelling v_η

A similar procedure is employed to determine the passive circuit components to represent v_η. The η-shaped component of v_{rect} can be defined in the time domain by substituting (11) into (17) resulting in

$$v_\eta = \begin{cases} -2V_b + \dfrac{I_{in}}{2\pi f_s C_p}(1 - \cos(\theta)) & \theta = 0 \ldots \theta_1 \\ 0 & \theta = \theta_1 \ldots \pi \\ 2V_b + \dfrac{I_{in}}{2\pi f_s C_p}(1 + \cos(\theta)) & \theta = \pi \ldots \pi + \theta_1 \\ 0 & \theta = \pi + \theta_1 \ldots 2\pi \end{cases} \tag{21}$$

The fundamental of (21) gives the FMA equivalent voltage source due to the η-shaped component of the rectifier voltage waveform

$$\begin{aligned} V_\eta = &\frac{1}{2\pi}\left(\int_0^{\theta_1}\left(-2V_b + \frac{I_{in}}{2\pi f_s C_p}(1 - \cos(\theta))\right)\sin(\theta)d\theta\right. \\ &\left.+ \int_{\pi}^{\pi+\theta_1}\left(2V_b + \frac{I_{in}}{2\pi f_s C_p}(1 + \cos(\theta))\right)\sin(\theta)d\theta\right) \\ &+ \frac{j}{2\pi}\left(\int_0^{\theta_1}\left(-2V_b + \frac{I_{in}}{2\pi f_s C_p}(1 - \cos(\theta))\right)\cos(\theta)d\theta\right. \\ &\left.+ \int_{\pi}^{\pi+\theta_1}\left(2V_b + \frac{I_{in}}{2\pi f_s C_p}(1 + \cos(\theta))\right)\cos(\theta)d\theta\right) \end{aligned}$$

which, after expanding the integrals and simplifying, reduces to

$$V_\eta = \frac{4V_b}{\pi}(\cos(\theta_1) - 1) - j\frac{4V_b}{\pi}\sin(\theta_1) \tag{22}$$

The real part of V_η can be utilised by substituting (9) into (22) to give

$$\begin{aligned} \mathrm{Re}(V_\eta) = &\frac{-32 f_s C_p V_{diode}(4\pi V_{diode} R_L f_s C_p + \pi V_{diode} + 2I_{in}R_L)}{\pi I_{in}(1 + 4R_L f_s C_p)} \\ &- \frac{32 I_{in} f_s C_p R_L^2}{\pi^2(1 + 4R_L f_s C_p)^2} \end{aligned} \tag{23}$$

and an equivalent passive resistor, r_η, can be subsequently obtained by dividing (23) by I_{in} (i.e. $r_\eta = V_\eta / I_{in}$)

$$\begin{aligned} r_\eta = &\frac{-32 f_s C_p V_{diode}(4\pi V_{diode} R_L f_s C_p + \pi V_{diode} + 2I_{in}R_L)}{\pi I_{in}^2(1 + 4R_L f_s C_p)} \\ &- \frac{32 f C_p R_L^2}{\pi^2(1 + 4R_L f_s C_p)^2} \end{aligned} \tag{24}$$

The imaginary part of (22) can also be expressed in terms of passive component parameters by substituting (9) into (22), although simple trigonometry can also be used to directly find $\sin(\theta_1)$, to give

$$\begin{aligned} \mathrm{Im}(V_\eta) = &-\frac{16 V_{diode}\gamma_2(4 f_s C_p R_L + 1}{\pi I_{in}(1 + 4R_L f_s C_p)^2} \cdots \\ &\frac{8 f C_p R_L(2\gamma_2 + \pi I_{in} + 2\pi f_s C_p R_L I_{in} - 2 f_s C_p R_L I_{in}\gamma_1}{2\pi^2 f_s C_p(1 + 4R_L f_s C_p)^2} \\ &\frac{-I_{in}\gamma_1) + (\pi I_{in} - I_{in}\gamma_1 - 4\gamma_2)}{} \end{aligned}$$

where

$$\gamma_1 = \cos^{-1}\left(\frac{32\pi f_s^2 C_p^2 V_{diode} R_L + 8\pi f_s C_p V_{diode} + 4 f_s C_p R_L I_{in} - I_{in}}{I_{in}(1 + 4R_L f_s C_p)}\right)$$

$$\gamma_2 = \sqrt{\frac{-f_s C_p (R_L I_{in} + \pi V_{diode} + 4\pi V_{diode} R_L f_s C_p)}{(16\pi f_s^2 C_p^2 V_{diode} R_L + 4\pi f_s C_p V_{diode} - I_{in})}} \tag{25}$$

Finally, an equivalent capacitance, c_η, can be derived

$$c_\eta = \frac{\pi I_{in}^2 C_p (16 f_s^2 C_p^2 R_L^2 + 8 f_s C_p R_L + 1)}{\left(\begin{array}{l}(16 I_{in}^2 R_L^2 (\pi - \gamma_1) + 128\pi\gamma_2 R_L V_{diode}) C_p^2 f_s^2 \ldots + ((8 I_{in}^2 (\pi - \gamma_1) \\ +16 I_{in}\gamma_2) R_L + 32\pi V_{diode}\gamma_2) C_p f_s + (\pi - \gamma_1) I_{in}^2 - 4\gamma_2 I_{in}\end{array}\right)} \tag{26}$$

5 Circuit analysis

Although the formulation of equivalent circuit parameters (c_η, r_η, r_{sq}) is useful for both circuit synthesis and nonlinear observer design, the dependence of their calculation on a knowledge of I_{in} is problematic for an analysis tool, since it is rarely known a-priori. By neglecting the diode characteristics, however, a linear approximation to the component values can be found, allowing an initial estimate of the input current to be made. Substituting $V_{diode} = 0$ into (20), (24) and (26), 'initial estimates' (denoted with a prime) of the equivalent component values are given by

$$r'_{eq} = r_{sq} + r_\eta = \frac{8R_L}{\pi^2(1 + 4R_L f_s C_p)^2}$$
$$c'_\eta = \frac{\pi C_P \gamma_3^2}{4\gamma_4\sqrt{f_s C_p R_L} + \pi\gamma_3^2 - \gamma_3^2 \cos^{-1}\left(\frac{\gamma_4}{\gamma_3}\right)} \tag{27}$$

where $\gamma_3 = 4 f_s C_p R_L + 1$, $\gamma_4 = 4 f_s C_p R_L - 1$, whilst an initial estimate of the total series capacitance of the resonant network is given by

$$C'_{tot} = \frac{C_s c'_\eta}{C_s + c'_\eta} \tag{28}$$

allowing the magnitude of the input current to be estimated from

$$|I'_{in}| = \frac{2V_{DC}}{\pi\sqrt{r'^2_{eq} + \left(\frac{(f_s^2/f_0^2) - 1}{2\pi f C'_{tot}}\right)^2}} \tag{29}$$

Equations (27)–(29) can be subsequently employed to generate an initial f_s against I_{in} characteristic, from which the output voltage can be obtained from (14). The estimates can subsequently be refined by iteration, as follows:

(i) Substitute $|I'_{in}|$ into (20), (24) and (26) to find equivalent component values

(ii) Substitute the calculated component values into (29) to find a more accurate value for $|I_{in}|$

(iii) Return to (i) for next iteration or, after a specified number of iterations, go to (iv)

(iv) Substitute $|I_{in}|$ into (15) to find the output voltage. The input current phase angle is also obtained from the phase angle of $1/Z_{res}$, where Z_{res} is the impedance of the equivalent resonant circuit, and is given by

$$Z_{res} = r_\eta + r_{sq} + \frac{j}{2\pi f_s C_{tot}}(2\pi f_s L_s C_{tot} - 1).$$

Numerous simulation studies have shown that convergence towards accurate solutions is rapid, with very little improvement in the results after a second iteration of the algorithm. By way of example, Fig. 7 compares results from time-domain SPICE [6] simulations of a 50–90 V converter of the type shown in Fig. 1, with initial and subsequently refined estimates of the output voltage from the converter. As is evident, results from the proposed method converge rapidly towards the SPICE results. Figure 7 also shows the results of a simple FMA analysis, and it can be seen that the proposed analysis method offers considerably more accurate results, with a similar processing time.

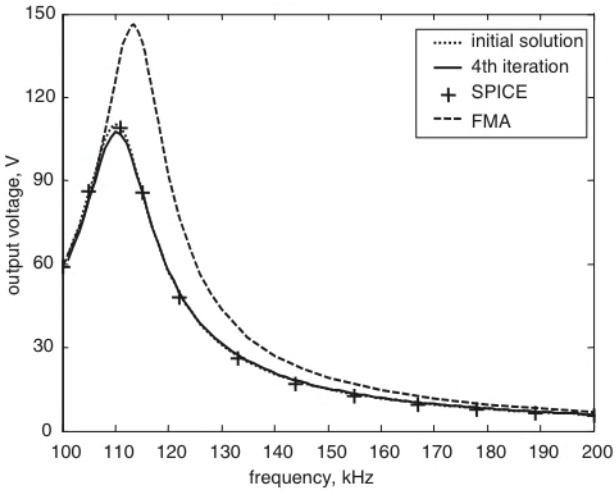

Fig. 7 *Converter output voltage characteristic*

5.1 Consequences of the analysis procedure

The process of rectifier transformation (as presented) of the three-element LCC converter yields a second-order circuit with a series capacitor and load resistance that are dependent on the switching frequency, f_s, and the load. This implies that the classical characteristics of the resulting second-order equivalent circuit (Fig. 4) are not constant, but are highly dependent on how the converter is excited. A major consequence of this is that the effective resonant frequency (f_{0eff}) of the system (30) is a function of the load, due to its dependence on the effective series capacitance, C_{tot}

$$f_{0eff}(f_s) = \frac{1}{2\pi}\sqrt{\frac{1}{L_s C_{tot}(f_s)}} \tag{30}$$

The effective quality factor of the transformed circuit, Q_{eff}, also contains terms that are dependent on the effective resistance and the effective capacitance, as follows:

$$Q_{eff} = \left(\frac{1}{r_\eta + r_{sq}}\right)\sqrt{\frac{L_s}{C_{tot}}} \tag{31}$$

Moreover, since characteristically, $r_{sq} < r_l$, and $r_\eta < 0$, Q_{eff} is generally higher than the series Q of the original L_s and C_s circuit, although the effect is somewhat offset by the reduction in C_{tot} compared to C_s. Similarly, the effective characteristic impedance, Z_{eff} (32), of the resonant network, is influenced by the equivalent rectifier action, $C_{tot} < C_s \Rightarrow Z_{eff} < Z_s$, which implies that the power transferred

by the series components can be increased

$$Z_{eff} = \sqrt{\frac{L_s}{C_{tot}}} \tag{32}$$

This should be borne in mind when selecting the series components in order that a converter with acceptable component stresses and correct power flow, can be realised. In general, this means that a larger series inductance and a smaller series capacitance will be required for an LCC voltage output converter compared to those for an 'equivalent' LC series voltage output converter.

6 Experimental verification of methodology

To demonstrate the accuracy of the proposed analysis technique, a prototype converter with a 25 V input, a fixed series impedance (31 Ω), and a variable load ($R_L = 5\ \Omega \ldots 85\ \Omega$), was designed to accommodate various values of the capacitor C_p.

The iterative procedure from Section 5 was used to estimate the output voltage of the converter for various values of C_p. Both initial estimates and refined estimates of V_{out} (after two iterations), are shown in Fig. 8. As will be seen, there is a high degree of correspondence between the predicted and measured results, particularly around the resonant frequency where other techniques of analysis can be particularly prone to error.

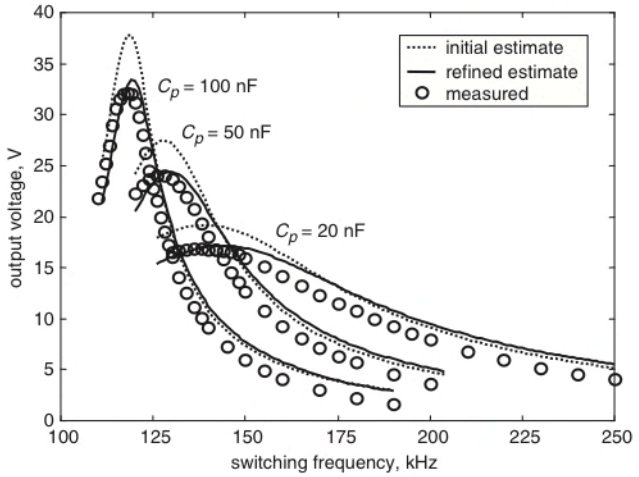

Fig. 8 *Switching frequency sweep*

6.1 Prediction of maximum output voltage: boost operation

Inspection of Fig. 8 reveals that when $C_p = 100$ nF the LCC voltage output converter exhibits a boost feature, which is not accurately predicted by any previously published analysis technique. For low values of C_p/C_s, the converter behaves in a similar manner to a second-order series LC converter, however, as the ratio of C_p/C_s is increased, the output voltage around the resonant frequency also increases until boost operation is achieved.

Ultimately, the phase difference between the input voltage and input current determines the voltage gain of the converter, with maximum output voltage occurring when the input voltage is in phase with the input current i.e. at resonance. Since the effective resonant frequency of the circuit has been shown to be a function of the load, and dV_{out}/df_s is highly dependent on Q_{eff}, an investigation of the maximum voltage gain of the converter for specified ratios of C_p/C_s and load resistance must be preceded by the determination of the effective resonant frequency, f_{0eff}. However, the complex interrelationship between the rate-of-change of the input phase angle, with respect to the frequency ($-d\angle Z_{res}/df_s$) impacts on numerical stability when calculating the maximum possible output voltage, particularly for systems which exhibit a high boost capability. A quasi-Newton frequency tuning procedure, based on the rate-of-change of frequency with phase difference, is therefore employed in an iterative manner, as follows:

$$f_{s(n+1)} = f_{s(n)} + \frac{k(\theta_T - \theta_A) f_{s(n)}}{Q_{eff(n)}}$$

where k is a constant to prevent overshoot (if the angles are expressed in radians, it can simply be set to 0.5), θ_T is the target phase angle (0 radians at the resonant frequency), θ_A is the actual phase angle ($-\angle Z_{res}$), and $f_{s(n)}$ is the switching frequency used in the preceding iteration.

Figure 9 shows the effect of varying the load resistance on the predicted maximum output voltage for three converter designs ($C_p = 20$, 50, 100 nF), using the quasi-Newton frequency tuning procedure to obtain the effective resonant frequency, f_{0eff}, for each converter at each load. Since the maximum output voltage occurs when the input voltage and current are in phase, Fig. 9 depicts operation of the converters under constant phase angle control. It is therefore seen that the maximum attainable output voltage increases with increasing C_p, implying that the power delivered to the load increases at the expense of a higher input current and increased component stresses. Further, the agreement between the predicted and measured results confirms the accuracy of the analysis.

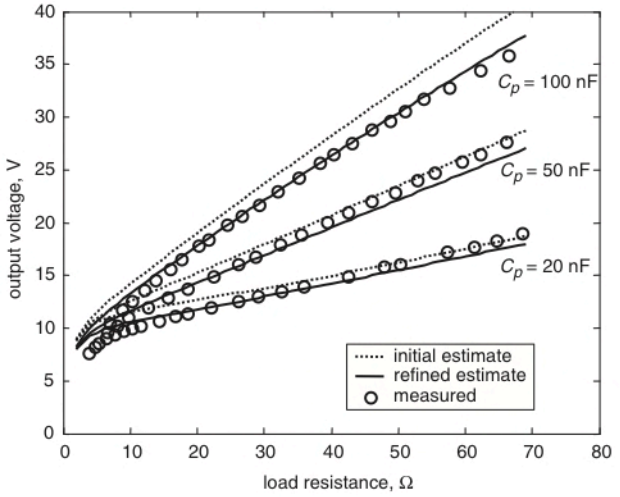

Fig. 9 *Variation of maximum output voltage with load resistance* achieved by adjusting switching frequency to gain maximum output voltage

Finally, Fig. 10 compares the measured and predicted output voltages when the switching frequency is set to provide maximum output voltage at the maximum load resistance, for each of the three converters. This, therefore, constitutes a fixed-frequency analysis of each converter, and, again, it is seen that the proposed analysis procedure yields good predictions of converter behaviour. Furthermore, although Figs. 9 and 10 appear qualitatively very similar, it is interesting to note that a comparison of the relative gradients of the characteristics shown, illustrates that fixed frequency operation of this converter topology imparts a higher Thévenin impedance to the converter when compared to operating the system at a fixed phase angle between the input voltage and input current.

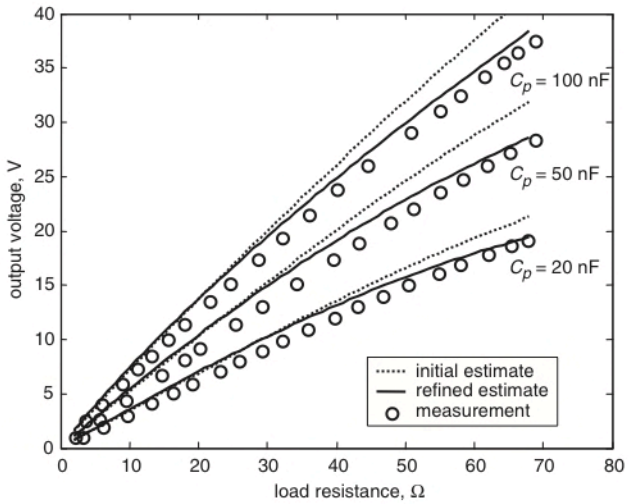

Fig. 10 *Variation of output voltage with load resistance* fixed switching frequency

7 Conclusions

The paper has described a methodology for the high speed analysis of LCC voltage output resonant power converters based on the derivation of describing functions to model the complex interactions between the bridge rectifier, the load, the output filter and the parallel rectifier capacitor. Subsequent transformation of the describing functions results in a passive network representation of the converter that can be employed to predict voltages and currents. The analysis procedure has also been shown to be enhanced by a refinement algorithm.

Predictions of the maximum output voltage as a function of the load, and the regulation at a fixed switching frequency as a function of the parallel rectifier capacitance, have been compared with measurements on prototype LCC voltage output converters, including operation in the boost mode. They confirm that the proposed analysis methodology affords significant accuracy, particularly around the resonant frequency, where other previously published analysis methods are prone to error.

8 References

1 Steigerwald, R.L.: 'A comparison of half-bridge resonant converter topologies', *IEEE Trans. Power Electron.*, 1988, **3**, (2), pp. 174–182
2 Mandhana, O.P.: 'Computer aided analysis and design of load commutated resonant converters', *IEEE Power Electron. Spec. Conf. Rec.*, 1996, **1**, pp. 279–285
3 Raju, G.S.N., and Doradla, S.: 'An LCL resonant converter with PWM control-analysis, simulation, and implementation', *IEEE Trans. Power Electron.*, 1995, **10**, (2), pp. 164–174
4 Bhat, A.K.S., and Dewan, S.B.: 'Analysis and design of a high-frequency resonant converter using LCC-type commutation', *IEEE Trans. Power Electron.*, 1987, **2**, (4), pp. 291–300
5 Hayes, J.G., and Egan, M.G.: 'Rectifier-compensated fundaments mode approximation analysis of the series-parallel LCLC family of resonant converters with capacitive filter and voltage-source load', *IEEE Power Electron. Spec. Conf. Rec.*, 1999, **2**, pp. 1030–1036
6 UC Berkeley SPICE3f3, University of California, Berkeley, Berkeley, CA